Electrochemical study on an activated carbon cloth modified by cyclic voltammetry with polypyrrole/anthraquinone sulfonate and reduced graphene oxide as electrode for energy storage

J. Fernández [a], J. Bonastre [a], J. Molina [a], F. Cases [a, *]

[a] *Departamento de Ingeniería Textil y Papelera, Escuela Politécnica Superior de Alcoy, Universitat Politècnica de València, Plaza Ferrándiz y Carbonell, s/n, 03801 Alcoy,* Spain

Abstract

This work describes a two-step procedure for the electrochemical coating of reduced graphene oxide (RGO) and polypyrrole anthraquinone sulfonate (PPyAQS) onto an activated carbon cloth (ACC) by cyclic voltammetry (CV). The textile samples were characterized by CV, electrochemical impedance spectroscopy (EIS) and galvanostatic charge-discharge measurements using a sandwich-type (electrode/separator/electrode) cell designed to operate in three or two-electrode configurations. The presence of RGO onto the ACC surface optimized the electrosynthesis of PPyAQS and reinforced the stability of the polymer with the number of charge/discharge cycles. A retention capacity of 90% after 100 charge-discharge cycles together with an energy density of 7.8×10^{-4} W h cm^{-2} at a power density of 1.8×10^{-3} W cm^{-2} were obtained for the ACC/RGO/PPyAQS sample. The analyses by field emission scanning electron microscopy (FESEM) showed the RGO veils-like and PPyAQS glomerular structures covering the ACC-fibers. The Fourier transform infrared spectroscopy (FTIR) analyses not only detected the presence of PPy and AQS, but also, the changes in the molecular

structure of PPyAQS, depending on its oxidation state, as consequence of the redox reactions occurred in the charge/discharge processes in the two-electrode cell.

Keywords: Activated carbon cloth; reduced graphene oxide; polypyrrole; anthraquinone sulfonate; electrochemical capacitor.

* Corresponding author. Tel.: +34 96 652 84 12; fax: +34 96 652 84 38.

E-mail address: fjcases@txp.upv.es (F. Cases).

1. Introduction

Among all the carbon-based substrates, ACC is a potential cheap material to be used as current collector for supercapacitors due to its unique structure, high surface area, good chemical stability, electrical conductivity and dimensional versatility [1]. In accordance with its high surface area, ACC presents a relatively high performance for the energy storage governed by the formation of the electrochemical double layer capacitance (EDLC) (non-faradaic mechanism) and in more or less extent, depending of the amount and kind of functional groups, by the redox reactions of those groups (faradaic mechanism) [2-6]. On the contrary, another group of materials, known as pseudocapacitors, based on transition metal oxides (MOx) [7-10] and conducting polymers (CPs) [11, 14] show very high capacitance behavior. Polypyrrole (PPy) is an intrinsically conducting polymer with high redox and capacitive current, high conductivity, high storage ability and good thermal and environmental stability (all these in a wide pH range) [15-17]. The main drawback of conducting polymers as electrodes for supercapacitors is their poor cycling stability because of swelling and shrinkage during doping/dedoping processes. Combinations of conducting polymer with

carbon materials have been attempted to reinforce the stability of the polymer as well as to improve the capacitance and conductivity of carbon-based supercapacitors [18]. Graphene is considered a unique material due to its electronic properties (high electron mobility at room temperature and ability to sustain high electric currents densities), mechanical properties, high specific surface area, etc. [19-21]. Moreover, reduced graphene oxide (RGO) possesses a large number of conjugated rings which can interact with porous carbon materials, but also many functional groups that can chemically interact with conducting polymers [22]. A number of composite materials based on PPy combined with graphene compounds [23-27] or carbon fibrous structures [28-31] have been demonstrated, showing highly stable capacitive performance. This is mainly attributed to the enhanced conductivity and/or redox behavior of the CPs-composites by carbon material integration. The electrical properties of PPy also depend on the size of the counter-ion. To prevent the expulsion of the counter-ion from the polymer structure (dedoping), organic anions with high molecular size such as anthraquinone sulfonate acid (AQSA), dodecylbenzene sulfonic acid (DBSA), naphtalensulfonic (NSA) acid, naphtalendisulfonic (NDSA) acid and p-toluene sulfonic acid (PTSA) have been used [32,33]. Moreover, it has been demonstrated that AQS dopant can significantly improve the pseudocapacitive performance of PPy [34,35].

On the basis of the above, in the present study, the surface of an ACC was modified by coating of RGO and PPyAQS using an environmentally friendly technique such as CV. The use of textiles as substrate for electrodes brings significant advantages related to their high surface/weight and surface/volume rates and dimensional versatility for the design of electrodes for electrochemical cells. The electrochemical behavior and the capability for energy storage of the modified textile electrodes were evaluated using a three or two-electrode cell configuration. The CV, EIS and the charge/discharge tests

were used for this purpose. FESEM and FTIR analyses were used to observe the morphology of different samples and to relate the molecular structure of PPyAQS with its oxidation state, respectively.

2. Experimental

2.1. Chemicals

Monolayer graphene oxide (GO) from Nanoinnova Technologies S.L. (Spain), lithium perchlorate and sulphuric acid from Merck, Pyrrole (98%) and sodium anthraquinone sulfonic salt (97%) from Sigma-Aldrich, were used as supplied. The solutions were prepared with ultrapure water (18.2 mΩ cm) from an Elix 3 Millipore-Milli-Q Advantage A10 system and deoxygenated by bubbling nitrogen gas (N_2 premier X50S).

2.2. Preparation of electrodes from ACC

The Zorflex® FM10 activated carbon cloth (0.5 mm thick with a surface density of 120 g m^{-2}) was provided by Chemviron Carbon. ACC strips of 1 cm x 3 cm were glued to 2 mm diameter copper rods with CircuitWorks® conductive epoxy resin. The resin was hardened at 85 ºC. Afterwards, the joint (ACC/resin/copper) was sealed with Teflon tape and glued with epoxy resin to isolate it from the solution. The copper rod was passed through a hollow glass rod. The electrodes so prepared were named with the abbreviation WE-ACCs.

2.3. Electrochemical cells

The CV syntheses with WE-ACCs were carried out using a voltammetric cone-shaped cell. The counter electrodes (CEs) were a Pt cylindrical mesh (6 cm height and 3 cm diameter) for the RGO-synthesis and a stainless steel cylindrical mesh (4 cm height and

3 cm diameter) for the polymerization of Py. The reference electrode was Ag/AgCl (3 M KCl). The WE-ACCs were put in the center of the cylinders and 3 cm^2 (geometric area) was introduced into the solutions of synthesis. The 3 g L^{-1} GO/0.1 M $LiClO_4 \cdot 3H_2O$ and 0.2 M Py/0.03 M AQS solutions were prepared by sonication for 30 and 40 minutes to disperse the GO monolayer powders and to dissolve the AQS salt, respectively.

During the synthesis the RGO, the GO solution was gently agitated with the aid of a magnetic stirrer to avoid the precipitation of GO.

For the electrochemical characterization of the textile samples (modified or not), small pieces of 0.5 cm x 0.5 cm were accurately cut from the WE-ACCs. A test-cell (Swagelok-type cell) ECC-Aqu from EL-CELL was employed. The electrical parts of the cell are made of gold. The samples (0.5 cm x 0.5 cm) were positioned on both sides of a glass fiber filter (2 cm diameter, 0.3 cm thick and 1.2 μm nominal pore size) soaked with a 0.1 M H_2SO_4 solution. Two circular gold discs (2 cm diameter) act as current collectors. For the experiments carried out in the three-electrode configuration, a gold metal pin, positioned between the two collectors, was used as the reference electrode (RE). The RE potential was +0.4 V vs. Ag/AgCl (3 M Ag/AgCl) under the experimental conditions. For the two-electrode configuration, the Au-pin terminal was unconnected and the RE-cable of the Autolab PGSTAT302 was connected to that of the counter electrode (CE).

2.4. Procedures: Synthesis and characterization

As the WE-ACCs presented a certain internal resistance and experienced a fast drop of current during both RGO and PPyAQS syntheses, CV was chosen with the purpose of

coating a significant amount of RGO and PPyAQS onto the ACC surface. The ohmic drop of the WE-ACCs was measured and introduced in the software of the Autolab.

The voltammetric parameters for the synthesis of RGO were established from a previous study [36] (not included) using a glassy carbon (GC) as working electrode since the voltammogram for WE-ACC did not show characteristic peaks. Accordingly, a potential range from -1.60 V to 0.60 V for 15 cycles at a scan rate of 10 mV s^{-1} was selected. The presence of an effective and significant amount of RGO was demonstrated by electrochemical and FESEM analyses.

The syntheses of PPyAQSn (where n is the number of cycles) with WE-ACC were carried out between 0.2 V and 1.3 V or 1.6 V vs. Ag/AgCl (3 M Ag/AgCl). A range from 0.2 V to 1.6 V vs. Ag/AgCl (3 M Ag/AgCl) was selected for WE-ACC/RGO15. Both syntheses were carried out at scan rates of 5 mV s^{-1}. The influence of the scan rate on the electrochemical response of PPyAQS has been proven. Low scan rates between 1 and 5 mV s^{-1} permit the charge transfer between substrate/polymer interface and along the PPy chains [32].

For the characterization by CV of the different samples in the three-electrode cell, a potential range between -0.9 V and 0.3 V vs. Au (0.1 M H_2SO_4), at a scan rate of 2.5 mV s-1, was used. To establish the voltage of the cell in the two-electrode configuration, the potential range established for the working electrode in the three-electrode configuration was taken into account. According to this, the potential of the two-electrodes was individually measured with the help of two digital multimeters, one of which was connected to WE:Au-pin terminals and the other to CE:Au-pin terminals. This procedure was carried out to know the variation of the potential of each electrode during the scanning of the cell voltage. Accordingly, a cell voltage between -1.25 V and 0.5 V was chosen for the experiments with the cell in the two-electrode configuration.

The charge/discharge currents of 1 mA (4 mA cm^{-2}) and 0.5 mA (2 mA cm^2) for the three and two-electrode cells, respectively, were obtained from the stabilized voltammograms in the Figs. 2b and 6. Two density currents of 8 and 4 mA cm^2 were also tested but a significant a loss of performance for the PPyAQS samples was observed. The low cyclability rate of PPyAQS-samples is a characteristic behavior of PPyAQS [32]. For the characterization by EIS of ACC, ACC/RGO_{15}, ACC/$PPyAQS_8$ and ACC/RGO_{15}/$PPyAQS_4$, the three-electrode configuration was chosen and a frequency range from 10^5 to 10^{-2} Hz was established.

2.5. Surface morphology and chemical structure characterization

For the FESEM analyses a Zeiss Ultra 55 microscope at a voltage of 3 kV was used. The FTIR-spectra were recorded after 400 scans at 4 cm^{-1} with a spectrophotometer FTIR NICOLET 6700 equipped with a horizontal-ATR accessory of zinc selenide.

3. Results and discussion

3.1. Characterization of ACC/RGO (three-electrode configuration)

Fig. 1a shows the CV curve for an ACC/RGO15 sample. No characteristic peaks are easily distinguished. Thus, in order to confirm the presence of RGO, two FESEM micrographs are shown in Fig. 1b and c. In these figures, the RGO structures are shown as veils that completely cover the ACC-fibers. It is also possible to observe the characteristic wrinkled and kinked morphology of RGO structures.

3.2. Synthesis and electrochemical characterization of ACC/PPyAQSn samples (three-electrode configuration)

Fig. 2a shows the CV curves corresponding to the fourth and eighth cycles recorded during the synthesis of PPy onto WE-ACC and WE-ACC/RGO15 between 0.2 and 1.6 V, respectively. No noticeable plot changes were observed when the upper limit of potential was 1.3 V. Fig. 2b shows the CV curves obtained for the characterization of different samples after the PPyAQS synthesis. Two peaks ascribed to the reduction-oxidation of the polymer backbone are clearly identified [18,26,35]. The increment of the current peak for ACC/PPyAQS2 (1.3 V), ACC/PPyAQS4 (1.3 V) and ACC/PPyAQS8 (1.3 V) is easily noted. Smaller differences are observed for ACC/PPyAQS8 (1.3 V), ACC/RGO15/PPyAQS4 (1.6 V) and ACC/PPyAQS8 (1.6 V) which could indicate that a limit in the effective amount of polymer that has been synthesized is reached. When comparing these CV curves with that for ACC, it can be concluded that PPyAQS is effectively coating the fibers of ACC, even with only two cycles of synthesis. Thus, the voltammetric response from ACC/PPyAQSn samples should be mostly due to the redox processes concerning the polymer. In Fig. 2c, the CV curve for an ACC sample soaked with a 0.03 M AQS and 0.1 M H_2SO_4 solution is shown. Two characteristic peaks corresponding to the reduction-oxidation of the AQS are observed. Considering the position of these peaks, it is safe to assume that in the CV curves for the PPyAQS samples, the two AQS peaks appear overlapped with those for the reduction-oxidation of PPy backbone [18,26,35]. In Fig. 2d, the charge-discharge curves, obtained at charge/discharge currents of ±1 mA, for ACC, ACC/PPyAQS4 (1.3 V), ACC/PPyAQS8 (1.3 V), ACC/RGO15/PPyAQS4 (1.6 V) and ACC/PPyAQS8 (1.6 V) are shown. The capacitance was calculated by the equation $C = It/V$ where I is the discharged current (A), t is the discharge time (s) and V is the potential change during

the discharge process (V). The results of the capacitance, which are summarized in Table 1, are expressed in terms of geometric area (0.25 cm^2), that is, areal capacitance C_A (F cm^{-2}). The reasons to carry this out was based on the fact that it was not possible to accurately determine the weight of PPyAQS which is, as it can be seen in Fig. 2b, primarily responsible of the electrochemical response of ACC/PPyAQSn samples.

	Loaded synthesis charge (C)	**C_A (F cm^{-2})**
ACC	**0.0**	**2.6**
ACC/PPyAQS4 (1.3 V)	**6.8**	**2.7**
ACC/PPyAQS8 (1.3 V)	**15.8**	**3.4**
ACC/RGO15/PPyAQS4 (1.6 V)	**9.5**	**4.8**
ACC/PPyAQS8 (1.6 V)	**30.7**	**5.8**

Table. 1. Summary of the areal capacitances for a current density of 4 mA cm^{-2} in the three-electrode cell.

Accordingly, it can be observed that increasing the charge of synthesis during the Py polymerization resulted in higher amounts of polymer and increasing values of C_A although the initial capacitance of ACC could be reduced due to the blocking of certain percentage of porosity by the coating. It is interesting to note the high value of C_A obtained for the sample containing RGO at a lower charge of synthesis. This result could be due to the morphology of RGO/PPyAQS which improves its capacitive

properties. To verify this result, samples of ACC/PPyAQS8 (1.3 V), and ACC/RGO15/PPyAQS4 (1.6 V) were analyzed by FESEM.

Figs. 3a-c show the Nyquist and Bode plots for ACC, ACC/RGO15, ACC/ PPyAQS8 (1.3 V) and ACC/RGO15/PPyAQS4 (1.6 V). A very different behavior between samples with and without PPyAQS is clearly appreciated. The samples without PPyAQS show a characteristic capacitive behavior. In the Nyquist diagram (Fig. 3a) the vertical lines are indicative of such behavior. Accordingly, in the Bode diagram (Fig. 3b) the phase angle at the lowest frequencies appears around -75 degrees. On the other hand, the PPyAQS samples show a significant diffusive behavior. This fact can be justified by the near 45 degrees slopes observed for PPyAQS8 (1.3 V) and ACC/RGO15/PPyAQS4 (1.6 V) in the Nyquist diagram of Fig. 3a. On that basis, the phase angle in the Bode diagram (Fig. 3b) is around to -50 degrees. It can be concluded that PPyAQS8 (1.3 V) and ACC/RGO15/PPyAQS4 (1.6 V) present a significant diffusion impedance in comparison with the samples without PPyAQS. As it can be seen in the Bode plot (Fig. 3c), the impedance module (lowest frequencies) increased an order of magnitude in the PPyAQS samples in relation to the samples non-polymerized. In the Fig. 4a, an enlarged image of the Nyquist plot of Fig. 3a is shown. The capacitive loops correspond, probably, to charge transfer resistances and inner resistances (R_{ctin}) of the electrodes. It can be noted that although there are a significant variation among the electrolyte resistance values, the R_{ctin} values remain around 1-2 ohms (quite low resistance). Therefore, the interfacial and inner resistances were approximately the same for ACC, ACC/RGO15, ACC/ PPyAQS8 (1.3 V) and ACC/RGO15/PPyAQS4 (1.6 V). Since the PPyAQS samples show high diffusion impedance, it was considered appropriate to perform EIS at a potential where PPyAQS was in an oxidized state. The Fig. 4b shows the Nyquist plots for ACC, ACC/RGO15, ACC/ PPyAQS8 (1.3 V) and

ACC/RGO15/PPyAQS4 (1.6 V) (the same as in Fig. 3a) but in the oxidized state at a potential of -0.485 V. It can be clearly observed how the diffusion impedance values decrease by an order of magnitude approximately when PPyAQS is in oxidized state. The values of the impedance module at lowest frequency (figure not shown) for ACC, ACC/RGO15, ACC/ PPyAQS8 (1.3 V) and ACC/RGO15/PPyAQS4 (1.6 V) were 47, 41, 42 and 32 Ω, respectively.

3.3. FESEM characterization

The FESEM micrographs of ACC/PPyAQS8 (1.3 V) and ACC/RGO15/PPyAQS4 (1.6 V) are shown in Figs. 5a-d. Figs. 5a and b, show the yarns of ACC coated uniformly by PPyAQS8 (1.3 V), which shows a glomerular structure. In Figs. 5c and d, PPyAQS4 structures coat uniformly the surface of ACC/RGO15. The size of the spherical particles of PPyAQS4 onto RGO15 (see Fig. 5d) appears reduced by roughly 50% in comparison to those onto the bare ACC surface (see Fig. 5b). According to this result, it can be concluded that RGO creates a more efficient distribution of PPyAQS which means an increment in the effective area of the ACC/RGO15/PPyAQS4. This result is coherent with the C_A values discussed in the above section.

3.4. Electrochemical study in a symmetric electrochemical capacitor (two-electrode cell configuration)

For the study in a real electrochemical capacitor, samples of ACC/PPyAQS8 (1.3 V) and ACC/RGO15/PPyAQS4 (1.6 V) were chosen to be tested in the symmetrical two-electrode cell. In a real storage device, the same material works in different potential ranges [37]. The stabilized voltammograms for ACC/PPyAQS8 (1.3 V) and ACC/RGO15/PPyAQS4 (1.6 V) are shown in Fig. 6. In accordance with these

voltammograms, it could be concluded that during the charge/discharge of the cell, faradic and non-faradaic processes are involved: the first ones are the faradaic reactions related to the oxidation/reduction of PPy; the second, the non-faradaic mechanism due to the formation of the double layer capacitance (EDLC). In Fig. 7a, the charge-discharge curves of ACC, ACC/PPyAQS8 (1.3 V) and ACC/RGO15/PPyAQS4 (1.6 V) are shown. These curves were obtained for a charge/discharge current of ±0.5 mA. The results expressed in terms of geometric area are summarized in the Table 2. The energy density was calculated according to the equation $ED = C(\Delta V)^2/2$ where C is the specific capacitance of the two-electrode cell and ΔV is the operating potential range. The averaged power density was calculated as $PD_{average} = ED/\Delta t$ where ED is the specific energy density and Δt the time of discharge of the cell.

	C_A (F cm^{-2})	ED_A (W h cm^{-2})	PD_A (W cm^{-2})
ACC	**1.3**	**$5.5\cdot10^{-4}$**	**$1.8\cdot10^{-3}$**
ACC/PPyAQS$_8$	**1.5**	**$6.5\cdot10^{-4}$**	**$1.8\cdot10^{-3}$**
ACC/RGO$_{15}$/PPyAQS$_4$	**1.8**	**$7.8\cdot10^{-4}$**	**$1.8\cdot10^{-3}$**

Table. 2. Areal values of capacitance (C_A), energy (ED_A) and power densities (PD_A) obtained with the two-electrode cell at 2 mA cm^{-2}.

According to the above, when the areal capacitance of the cell CA (F cm^{-2}) is calculated, the contribution of PPy-oxidation/reduction reactions is less than that for the three-electrode cell. For the three-electrode cell, the stabilized voltammograms were obtained for a range of potential which cover mainly the PPy-faradic reactions. That is why the differences between the CA values for non-modified and RGO/PPyAQS-modified

samples are smaller for the two-electrode cell. Nevertheless, increments of 15% and 38% were obtained for ACC/PPyAQS$_8$ and ACC/RGO$_{15}$/PPyAQS$_4$, respectively. It is interesting to note that the areal power densities of ACC, ACC/PPyAQS8 (1.3 V) and ACC/RGO15/PPyAQS4 (1.6 V) have about the same values, that is, same power output of the energy based on them. This result is in accordance with the fact that the charge transfer and inner resistances (Rcint) of these samples show similar values, around 1-2 ohms, which is a quite low value. The specific energy density for ACC/RGO15/PPyAQS4 (1.6 V) is higher than that for ACC/PPyAQS8 (1.3 V) which was synthesized at a higher loaded charge (see Table 1). In order to compare these results with those reported in the literature for textile supercapacitors, the Ragone plot reported by Changsoon Choi et al. [38] was taken as a reference. In this plot, the ED_A (W h cm^{-2}) values are established between 10^{-8} and 10^{-4} while the PD_A (W cm^{-2}) values are ranged from 10^{-6} to 10^{-2}. A novel cable-type flexible supercapacitor with excellent performance was fabricated using 3D PPy-MnO_2-CNT-cotton thread multi-grade nanostructures as electrodes by Nishuang Liu et al. [39]. The supercapacitors showed an areal energy density of 33 μW h cm^{-2} at a power density of 0.67 mW cm^{-2} and a high areal power density of 13 mW cm^{-2} at an energy density of 14.7 μW h cm^{-2}. From high capacitive MnO_2–PPy–carbon fiber and V_2O_5–PANI–carbon fiber composites, a flexible wire-shaped fiber asymmetric supercapacitor (WFASC) was fabricated by Weijie Liu et al. [40]. For a wide potential window of 2.0 V a high areal capacitance of 0.613 F cm^{-2} at a discharge current density of 1.5 mA cm^{-2} and a high energy density of 0.340 mW h cm^{-2} at a power density of 1.5 mW cm^{-2} were obtained. Thus, promising values of both areal energy and power densities are obtained in the present work.

In Fig. 7b the plot of the retention capacity versus number of charge/discharge cycles is shown. The stability of the sample with RGO is clearly visible, retaining 90% of its

capacitance. This result is coherent with the fact that the combination of conducting polymer with carbon materials reinforces the stability of the polymer as well as improving the capacitance of carbon-based supercapacitors [16]. A density current of 4 mA cm^2 was also tested. The values of C_A (F cm^{-2}) resulted in a significant loss of performance for ACC, ACC/$PPyAQS_8$ and ACC/RGO_{15}/$PPyAQS_4$ of 5.0%, 12.5% and 14.5%, respectively.

3.5. FTIR-analysis

The FTIR-spectrum of ACC was compared with the spectra of ACC/PPyAQS8 (1.6 V) and ACC/RGO15/PPyAQS4 (1.6 V) in Fig. 8a. The assignment of the bands is described below:

- The band centred at 708 cm^{-1} is associated to C-S stretching of the sulfonic group of AQS [41]. This band clearly appears in both samples coated with PPyAQS and RGO/PPyAQS
- A strong band between 1140-1080 cm^{-1} attributed to the stretching vibration of C-O bonds [42] appears clearly visible in the ACC-spectrum. The presence of PPyAQS and RGO/PPyAQS contributed to the modification of this band.
- The band centred at 1288 cm^{-1} is identified with the C-N bonds stretching vibration [42]. A more intense band is observed in the RGO/PPyAQS spectrum.
- A band centred at 1510 cm^{-1} attributed to C-C bonds stretching vibration in PPyAQS ring [42] is observed for both ACC/PPyAQS8 (1.6 V) and ACC/RGO15/PPyAQS4 (1.6 V) samples.
- An intense absorption band at around 1740 cm^{-1} is identified with the stretching vibration of the C=O bonds of anthraquinone group [43].

In Fig. 8b, the spectra of two 0.25 cm^{-2} samples of ACC/RGO15/PPyAQS4 (1.6 V), used in the stability tests with the two-electrode cell, are shown. Since the FTIR spectra are similar to these shown in Fig. 8a, it can be concluded that PPyAQS still remain on the surface of the electrode after the stability tests. On the other hand, according with the spectra, it is possible to observe their different redox state. In the sample ACC/RGO15/PPyAQS4 (1.6 V)ox, the band centred at around 1740 cm^{-1}, which is identified as the stretching vibration of the C=O bonds of the anthraquinone group, is visible. On the contrary, in the spectrum for ACC/RGO15/PPyAQS4 (1.6 V)red, this band has disappeared because of the reduction of the C=O bond and, consequently, a new band at 1117 cm^{-1} [42]. This band could be associated with the stretching vibration of the C-O bond from the reduction of the anthraquinone group. So, FTIR analysis not only detect the presence of PPy and AQS onto the ACC yarn after its synthesis and after 100 charge/discharge cycles, but also it is possible to monitor the PPy oxidation/reduction associated with the charge/discharge processes.

4. Conclusions

An ACC was successfully modified with RGO and PPyAQS by CV. EIS showed significant results for the supercapacitors based on PPyAQS and RGO/PPyAQS. The role of RGO in the synthesis of the polymer and the capacitance of the system has been demonstrated in the electrochemical and morphologic analyses. Thus, the combination of RGO with PPyAQS optimized the electrosynthesis of PPy, increased the areal capacitance and the energy density and reinforced the stability of the polymer with the number of charge/discharge cycles. The values of areal energy and power density of $7.8x10^{-4}$ W h cm^{-2} at $1.8x10^{-3}$ W cm^{-2} obtained in the present work are comparable to

those reported in the literature. So, promising results for capacitive applications in which electrodes with a high surface/low-volume rate is needed, have been achieved.

5. Acknowledgements

The authors wish to acknowledge to Chemviron Carbon who kindly donated the ZORFLEX® activated carbon fabric. The authors wish to thank the Spanish Agencia Estatal de Investigación de Economía (AEI) and European Union (FEDER funds) for the financial support (contract MAT2016-77742-C2-1-P). Tim Vickers is gratefully acknowledged for help with the English revision. Electron Microscopy Service of the UPV (Universitat Politècnica de València) is gratefully acknowledged for help with FESEM characterization.

6. Bibliography

[1] I. Shown, A. Ganguly, L-Ch. Chen, K-H. Chen, Conducting polymer-based flexible supercapacitor: a review, Energy Science & Engineering 3 (2015) 2−26.

[2] A.G. Pandolfo, A.F. Hollenkamp, Carbon properties and their role in supercapacitors, J. Power Sources 157 (2006) 11–27.

[3] E. Frackowiak, F.B. Béguin, Carbon materials for the electrochemical storage of energy in capacitors, Carbon 39 (2001) 937–950.

[4] T.-H. Wu, C.-T. Hsu, C.-C. Hu, L.J. Hardwick, Important parameters affecting the cell voltage of aqueous electrical double-layer capacitors, J. Power Sources 242 (2013) 289–298.

[5] H.P. Jiang, H.P.S. Lee, C. Li, 3D carbon based nanostructures for advanced supercapacitors, Energy Environ. Sci. 6 (2013) 41–53.

[6] A.J. Amali, J.-K. Sun, Q. Xu, From assembled metal-organic framework nanoparticles to hierarchically porous carbon for electrochemical energy storage, Chem. Commun. 50 (2014) 1519–1522.

[7] M.B. Sassin, C.N. Chervin, D.R. Rolison, J.W. Long, Redox deposition of nanoscale metal oxides on carbon for next-generation electrochemical capacitors, Acc. Chem. Res. 46 (2013) 1062–1074.

[8] M. Zhi, M.C. Xiang, J. Li, M. Li, N. Wu, Nanostructured carbon-metal oxide composite electrodes for supercapacitors: a review, Nanoscale 5 (2013) 72–88.

[9] Y. Yue, Zh. Yang, N. Liu, W. Liu, H. Zhang, Y. Ma, C. Yang, J. Su, L. Li, F. Long, Z. Zou, Y. Gao, A flexible integrated system containing a microsupercapacitor, a photodetector, and a wireless charging coil, ACS Nano 10 (2016) 11249–11257.

[10] N. Liu, Y. Gao, Recent progress in micro-supercapacitors with in-plane interdigital electrode architecture, Small 13 (2017) 1701189–1701199.

[11] K.R. Prasad, K. Koga, N. Miura, Electrochemical deposition of nanostructured indium oxide: high-performance electrode material for redox supercapacitors, Chem. Mater. 16 (2004) 1845–1847.

[12] M.P. Kalaji, P.J. Murphy, G.O. Williams, The study of conducting polymers for use as redox supercapacitors, Synth. Met. 102 (1999) 1360–1361.

[13] K. Wang, H. Wu, Y. Meng, Z. Wei, Conducting polymer nanowire arrays for high performance supercapacitors, Small 10 (2014) 14–31.

[14] T. Liu, L. Finn, M. Yu, H. Wang, T. Zhai, X. Lu, Polyaniline and polypyrrole pseudocapacitor electrodes with excellent cycling stability, Nano Lett. 14 (2014) 2522–2527.

[15] Q.W. Zhang, X. Zhou, H.-S. Yang, Capacitance properties of composites electrodes prepared by electrochemical polymerization of pyrrole on carbon foam in aqueous solution, J. Power Sources 125 (2004) 141–147.

[16] C. Li, H. Bai, G. Shi, Conducting polymer nanomaterials: electrosynthesis and applications, Chem. Soc. Rev. 38 (2009) 2397–2409.

[17] C. Xu, J. Sun, L. Gao, Synthesis of a novel hierarchical graphene/polypyrrole nanosheet composite and their superior electrochemical performance, J. Mater. Chem. 21 (2011) 11253–11258.

[18] S. Konwer, R. Boruah, S.K. Dolui, Studies on conducting polypyrrole/graphene oxide composites as supercapacitor electrode, J. Electron. Mater. 40(11) (2011) 2248–2255.

[19] A.K. Geim, K.S. Novoselov, The rise of graphene, Nat. Mater. 6 (2007) 183−191.

[20] K.S. Novoselov, A.K. Geim, S.V. Morozov, D. Jiang, Y. Zhang, S.V. Dubonos, A.A. Grigorieva, A.A. Firsov, Electric field effect in atomically thin carbon films, Science 306 (2004) 666−669.

[21] K.S. Novoselov, D. Jiang, F. Scheding, T.J. Booth, V.V. Khotkevich, S.V. Morozov, A.K. Geim, Two-dimensional atomic crystals, Proc. Natl. Acad. Sci. USA 102 (2005) 10451−10453

[22] M. Zhong, Y. Song, Y. Li, Ch. Ma, X. Zhai, J. Shi, Q. Guo, L. Liu, Effect of reduced graphene oxide on the properties of an activated carbon cloth/polyaniline flexible electrode for supercapacitors application, J. Power Sources 217 (2012) 6−12.

[23] S. Biswas, L.T. Drzal, Multilayered nanoarchitecture of graphene nanosheets and polypyrrole nanowires for high performance supercapacitor electrodes, Chem. Mater. 22 (2010) 5667–5671.

[24] Y. Zhao, J. Liu, Y. Hu, H. Cheng, C. Hu, C. Jiang, Highly compression-tolerant supercapacitor based on polypyrrole-mediated graphene foam electrodes, Adv. Mater. 25 (2013) 591–595.

[25] A. Davies, P. Audette, B. Farrow, F. Hassan, Z. Chen, J.-Y. Choi, Graphene-based flexible supercapacitors: pulse-electropolymerization of polypyrrole on free-standing graphene films, J. Phys. Chem. C 115 (2011) 17612–17620.

[26] Ch. Zhu, J. Zhai, D. Wen, S. Dong, Graphene oxide/polypyrrole nanocomposites: one-step electrochemical doping, coating and synergistic effect for energy storage, J. Mater. Chem. 22 (2012) 6300–6306.

[27] J. Zhang, P. Chen, B.H.L. Oh, M.B. Chan-Park, High capacitive performance of flexible and binder-free graphene-polypyrrole composite membrane based on in situ reduction of graphene oxide and self-assembly, Nanoscale 5 (2013) 9860–9866.

[28] A. Rudge, J. Davey, I. Raistrick, S. Gottesfeld, J.P. Ferraris, Conducting polymers as active materials in electrochemical applications, J. Power Sources 47 (1994) 89–107.

[29] A. Rudge, I. Raistrick, S. Gottesfeld, J.P. Ferraris, Study of the electrochemical properties of conducting polymers for applications in electrochemical capacitors, Electrochim. Acta 39 (1994) 273–287.

[30] J.-H. Kim, A.K. Sharma, Y.-S Lee, Synthesis of polypyrrole and nano-fiber composite for the electrode of electrochemical capacitor, Mater. Lett. 60 (2006) 1697–1701.

[31] B. Muthulakshmi, D. Kalpana, S. Pitchumani, N.G. Renganathan, Electrochemical deposition of polypyrrole for symmetric supercapacitors, J. Power Sources 158 (2016) 1533–1537.

[32] J. Molina, J. Fernández, A.I. del Río, R. Lapuente, J. Bonastre, F. Cases, Stability of conducting polyester/polypyrrole fabrics in different pH solutions. Chemical and electrochemical characterization, Polym. Degrad. Stab. 95 (2010) 2574–2583.

[33] S. Harish, D. Sridharan, S.S. Kumar, J. Joseph, K.L.N. Phani, Barrier films to control loss of 9,10-anthraquinone-2-sulphonate dopant from PEDOT films during electrochemical transitions, Electrochim. Acta 54(13) (2009) 3618–3622.

[34] X. Lang, Q. wang, Ch. Feng, X. Yue, W. Xu, J. Li, Sh. Fan, The role of anthraquinone sulfonate dopants in promoting performance of polypyrrole composites as pseudo-capacitive electrode materials, Synth. Met. 160 (2010) 1800-1804.

[35] Y. Yang, K. He, P. Yana, D. Wanga, X. Wua, X. Zhao, Z. Huang, Ch. Zhanga, D. Hea, Enhanced Capacity of Polypyrrole/Anthraquinone Sulfonate/Graphene Composite as Cathode in Lithium Batteries, Electrochim. Acta 138 (2014) 481–485.

[36] J. Fernández, J. Bonastre, J. Molina, A.I. del Río, F.J. Iborra, Study on the specific capacitance of an activated carbon cloth modified with reduced graphene oxide and polyaniline by cyclic voltammetry, Eur. Polym. J. 92 (2017) 194-203.

[37] V. Khomenko, E. Frackowiak, F. Béguin, Determination of the specific capacitance of conducting polymer/nanotubes composite electrodes using different cell configurations, Electrochim. Acta 50 (2005) 2499–2506.

[38] Ch. Choi, K.M. Kim, K.J. Kim, X. Lepró, G.M. Spinks, R.H. Baughman, S.J. Kim, Improvements of system capacitance via weavable superelastic biscrolled yarn supercapacitors, Nat. Commun. 7 13811 (2016).

[39] N. Liu, W. Ma, J. Tao, X. Zhang, J. Su, L. Li, C. Yang, Y. Gao, D. Golberg, Y. Bando, Cable-type supercapacitors of three-dimensional cotton thread based multi-grade nanostructures for wearable energy storage, Adv. Mater. 25 (2013) 4925–4931.

[40] W. Liu, N. Liu, Y. Shi, Y. Chen, C. Yang, J. Tao, S. Wang, Y. Wang, J. Su, L. Li, Y. Gao, A wire-shaped flexible asymmetric supercapacitor based on carbon fiber coated with a metal oxide and a polymer, J. Mater. Chem. A 3 (2015) 13461–13467.

[41] C. Hamtom, D. Demoin, R.E. Glaser, Vibrational spectroscopy tutorial: Sulfur and phosphorus, 2010. https://faculty.missouri.edu/~glaserr/8160f10/A03_Silver.pdf.

[42] A. Streitwieser, C.H. Heathcock, Química Orgánica, third ed., Interamericana McGraw-Hill, Spain, 1987.

[43] Ucla Department of Chemistry and Biochemistry, Problems in NMR and IR spectroscopy. https://webspectra.chem.ucla.edu/index.html.

Figure Captions

Fig. 1. (a) CV curve for ACC/RGO15 at a scan rate of 2.5 mV s^{-1}. (b) and (c) FESEM-micrographs for ACC/RGO15 at 5 Kx and 15 Kx.

Fig. 2. (a) CV curve for the PPy synthesis on WE-ACC and WE-ACC/RGO15 recorded in 0.2 M Py and 0.03 M AQS solution at 5 mV s^{-1}. (b) CV curves of ACC, ACC/PPyAQS2 (1.3 V), ACC/PPyAQS4 (1.3 V), ACC/PPyAQS8 (1.3 V), ACC/RGO15/PPyAQS4 (1.6 V) and ACC/PPyAQS8 (1.6 V) recorded at a scan rate of 2.5 mV s^{-1} for the three-electrode cell configuration in 0.1 M H_2SO_4 aqueous medium. (c) CV curve for an ACC soaked with the 0.03 M AQS and 0.1 M H_2SO_4 solution at 2.5 mV s^{-1}. (d) Charge/discharge curves for ACC, ACC/PPyAQS$_4$ (1.3 V), ACC/PPyAQS8 (1.3 V), ACC/RGO15/PPyAQS4 (1.6 V) and ACC/PPyAQS8 (1.6 V) obtained at charge/discharge currents of ±1mA.

Fig. 3. (a) Nyquist and (b, c) Bode plots for ACC, ACC/RGO15, ACC/PPyAQS8 (1.3 V) and ACC/RGO15/PPyAQS4 (1.6 V). Frequency range from 10^5 to 10^{-2} Hz. The open circuit potential was -0.1 V.

Fig. 4. (a) Enlarge image of Nyquist plot of Fig. 3a and (b) Nyquist plot for ACC, ACC/RGO15, ACC/PPyAQS8 (1.3 V) and ACC/RGO15/PPyAQS4 (1.6 V) in the oxidized state at -0.5 V. Frequency range from 10^5 to 10^{-2} Hz.

Fig. 5. (a) and (b) micrographs for ACC/PPyAQS8 (1.3 V) at 500 x and 15 Kx. (c) and (d) micrographs for ACC/RGO15/PPyAQS4 at 500 x and 15 Kx.

Fig. 6. Stabilized CV curves for ACC/PPyAQS8 (1.3 V) and ACC/RGO15/PPyAQS4 (1.6 V) recorded at a scan rate was 2.5 mV s^{-1} using the two-electrode configuration.

Fig. 7. (a) Charge/discharge curves for ACC, ACC/PPyAQS8 (1.3 V) and ACC/RGO15/PPyAQS4 (1.6 V) obtained at charge/discharge currents of ±0.5 mA. (b) Retention capacity versus cycle number for ACC, ACC/PPyAQS8 (1.3 V) and ACC/RGO15/PPyAQS4 (1.6 V) during 100 cycles (for 72 hours).

Fig. 8. (a) FTIR-spectra for ACC, ACC/RGO15/PPyAQS4 (1.6 V) and ACC/PPyAQS8 (1.6 V). (b) FTIR-spectra for two samples of ACC/RGO15/PPyAQS4 (1.6 V), in their oxidized or reduced state, taken after the 100 cycles stability test in the two-electrode cell. The spectra were recorded after 400 scans and a resolution of 4 cm^{-1}.

Tables

Table. 1. Summary of the areal capacitances for a current density of 4 mA cm^{-2} in the three-electrode cell.

Table. 2. Areal values of capacitance (C_A), energy (ED_A) and power densities (PD_A) obtained with the two-electrode cell at 2 mA cm^{-2}.

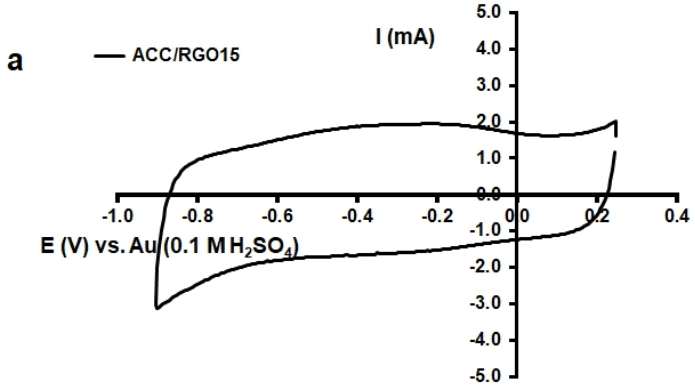
a
ACC/RGO15
I (mA)
5.0
4.0
3.0
2.0
1.0
0.0
-1.0
-2.0
-3.0
-4.0
-5.0
-1.0
-0.8
-0.6
-0.4
-0.2
0.0
0.2
0.4
E (V) vs. Au (0.1 M H_2SO_4)

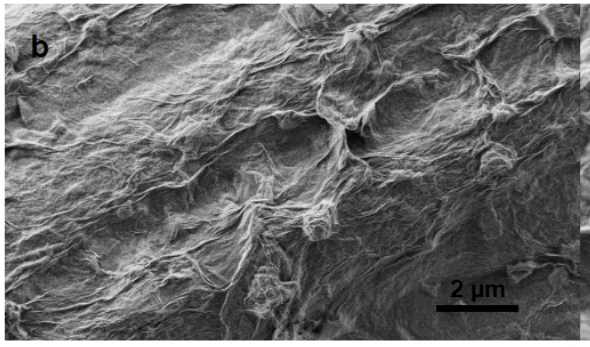
b
2 µm

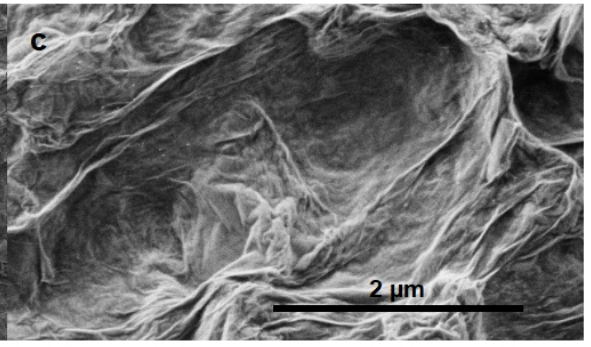
c
2 µm

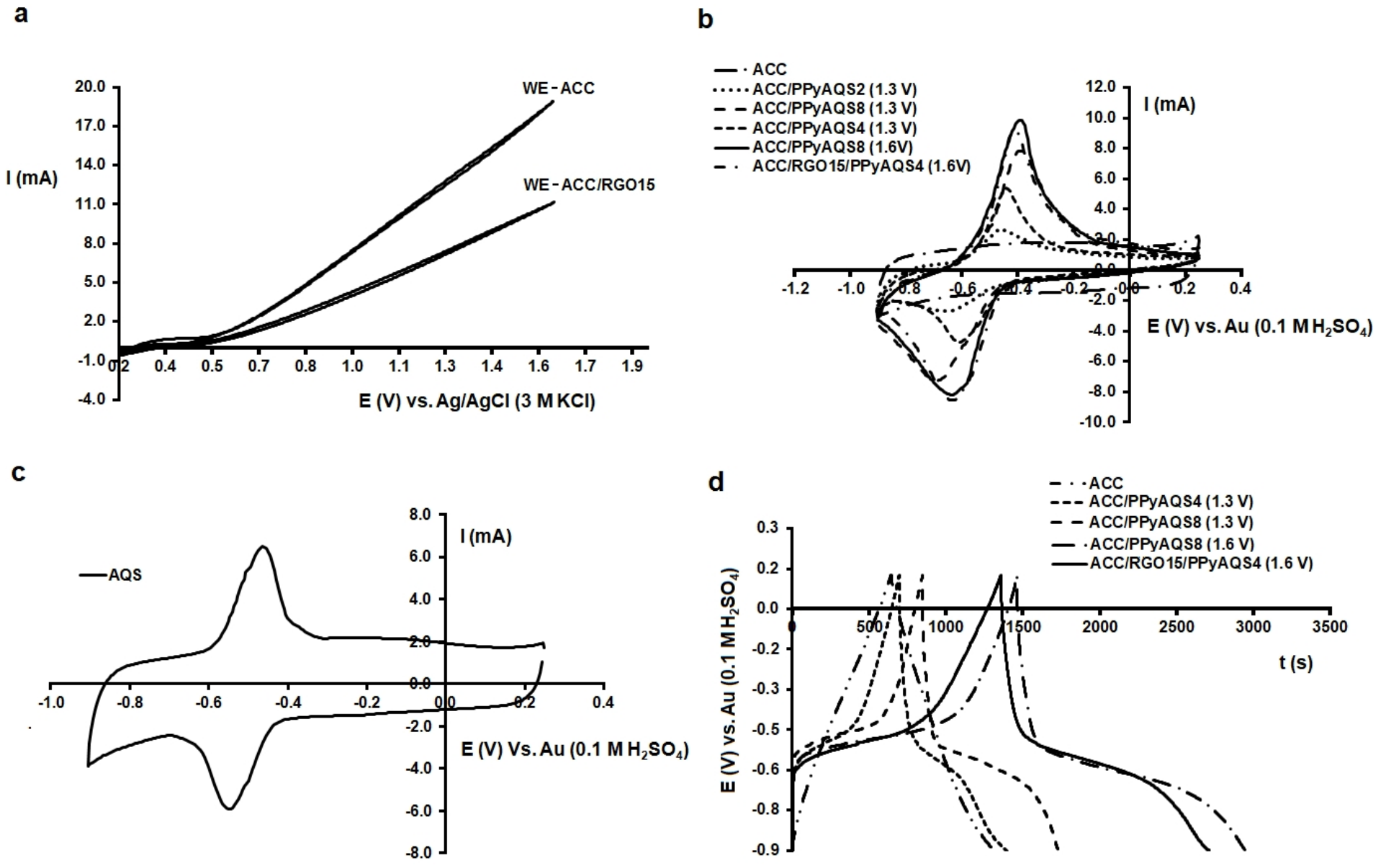
a
I (mA)
WE - ACC
WE - ACC/RGO15
E (V) vs. Ag/AgCl (3 M KCl)
b
ACC
ACC/PPyAQS2 (1.3 V)
ACC/PPyAQS8 (1.3 V)
ACC/PPyAQS4 (1.3 V)
ACC/PPyAQS8 (1.6V)
ACC/RGO15/PPyAQS4 (1.6V)
I (mA)
E (V) vs. Au (0.1 M H2SO4)
c
AQS
I (mA)
E (V) Vs. Au (0.1 M H2SO4)
d
ACC
ACC/PPyAQS4 (1.3 V)
ACC/PPyAQS8 (1.3 V)
ACC/PPyAQS8 (1.6 V)
ACC/RGO15/PPyAQS4 (1.6 V)
E (V) vs. Au (0.1 M H2SO4)
t (s)

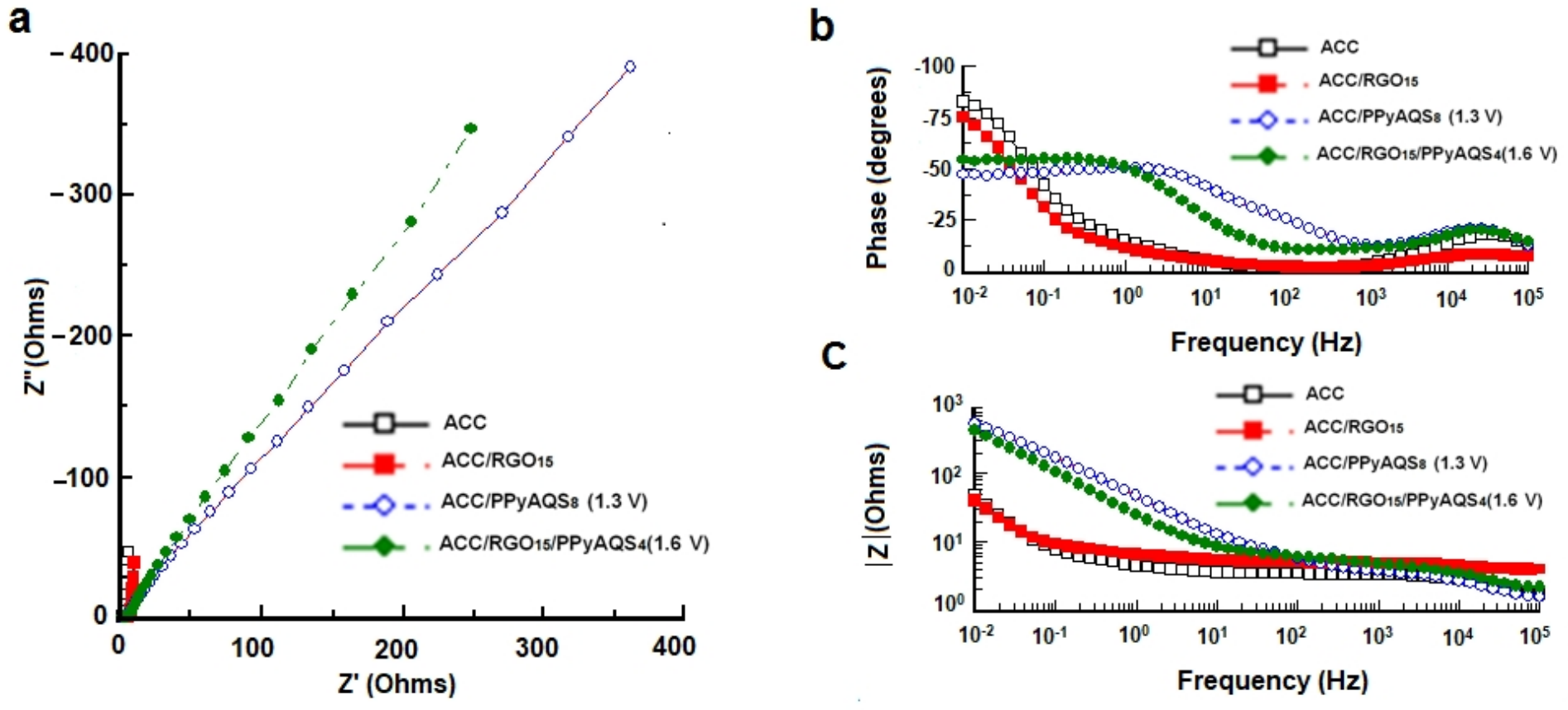
a
Z''(Ohms)
Z' (Ohms)
ACC
ACC/RGO15
ACC/PPyAQS8 (1.3 V)
ACC/RGO15/PPyAQS4(1.6 V)
b
Phase (degrees)
Frequency (Hz)
c
|Z|(Ohms)
Frequency (Hz)

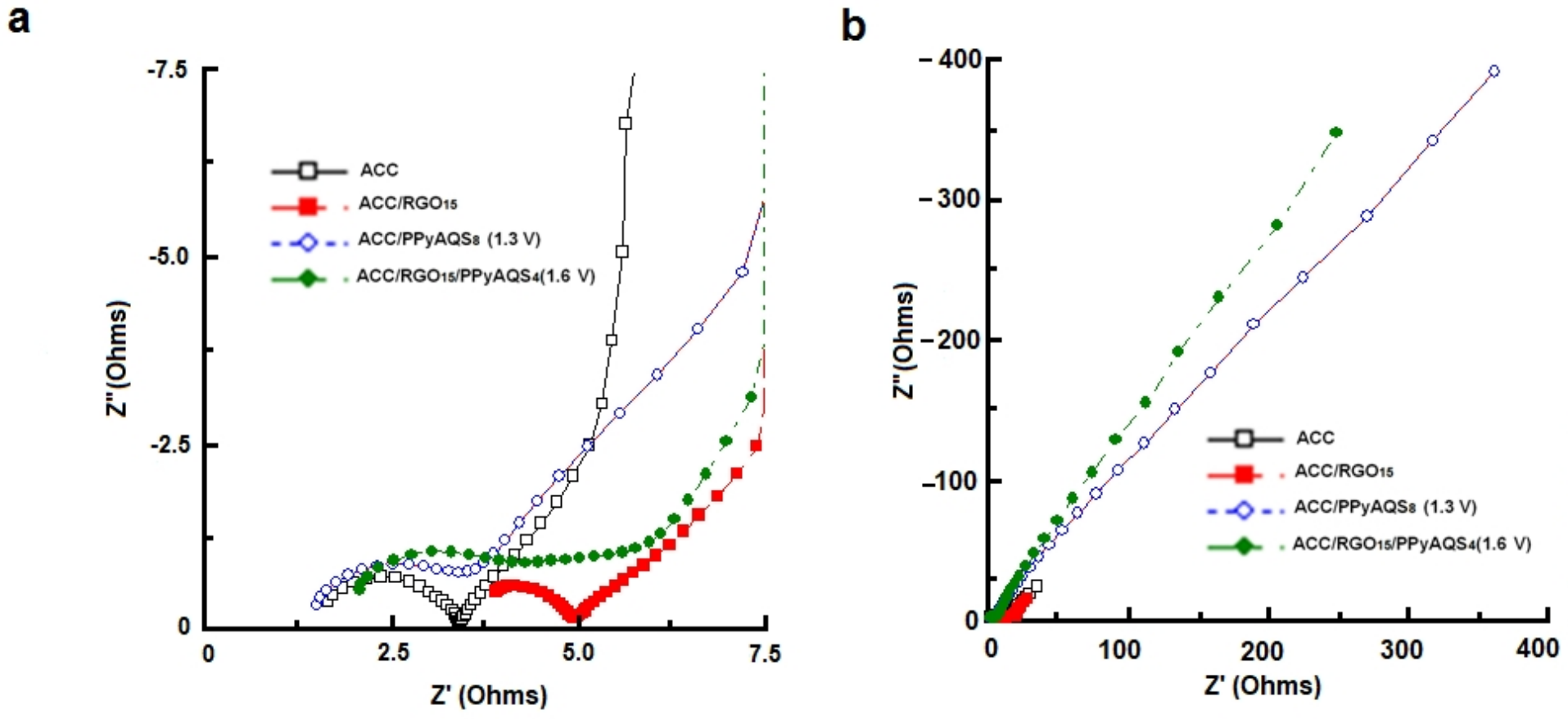
a
-7.5
-5.0
-2.5
0
Z''(Ohms)
0
2.5
5.0
7.5
Z' (Ohms)
ACC
ACC/RGO15
ACC/PPyAQS8 (1.3 V)
ACC/RGO15/PPyAQS4(1.6 V)
b
400
300
200
100
0
Z''(Ohms)
0
100
200
300
400
Z' (Ohms)
ACC
ACC/RGO15
ACC/PPyAQS8 (1.3 V)
ACC/RGO15/PPyAQS4(1.6 V)

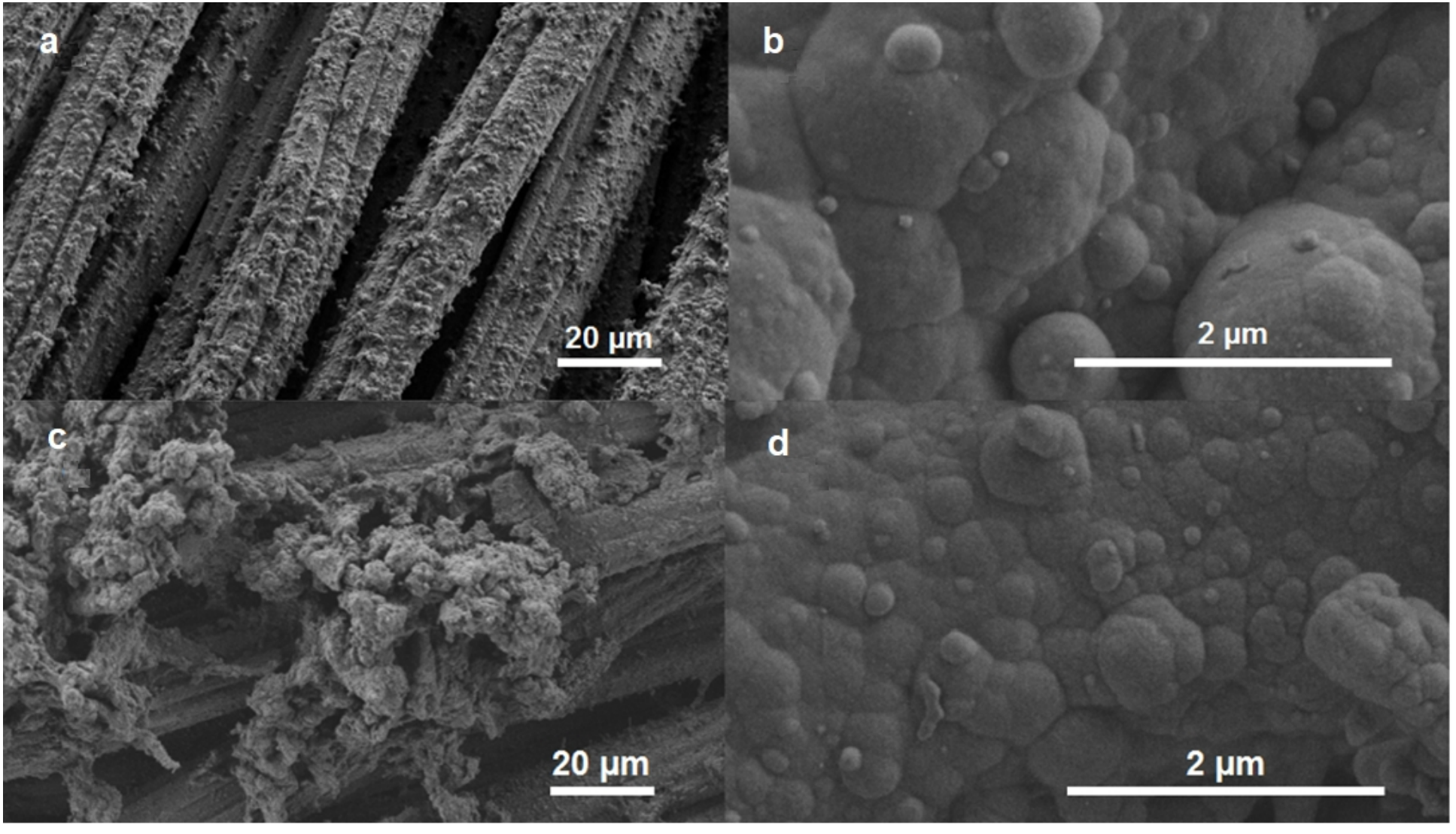
a
20 μm
b
2 μm
c
20 μm
d
2 μm

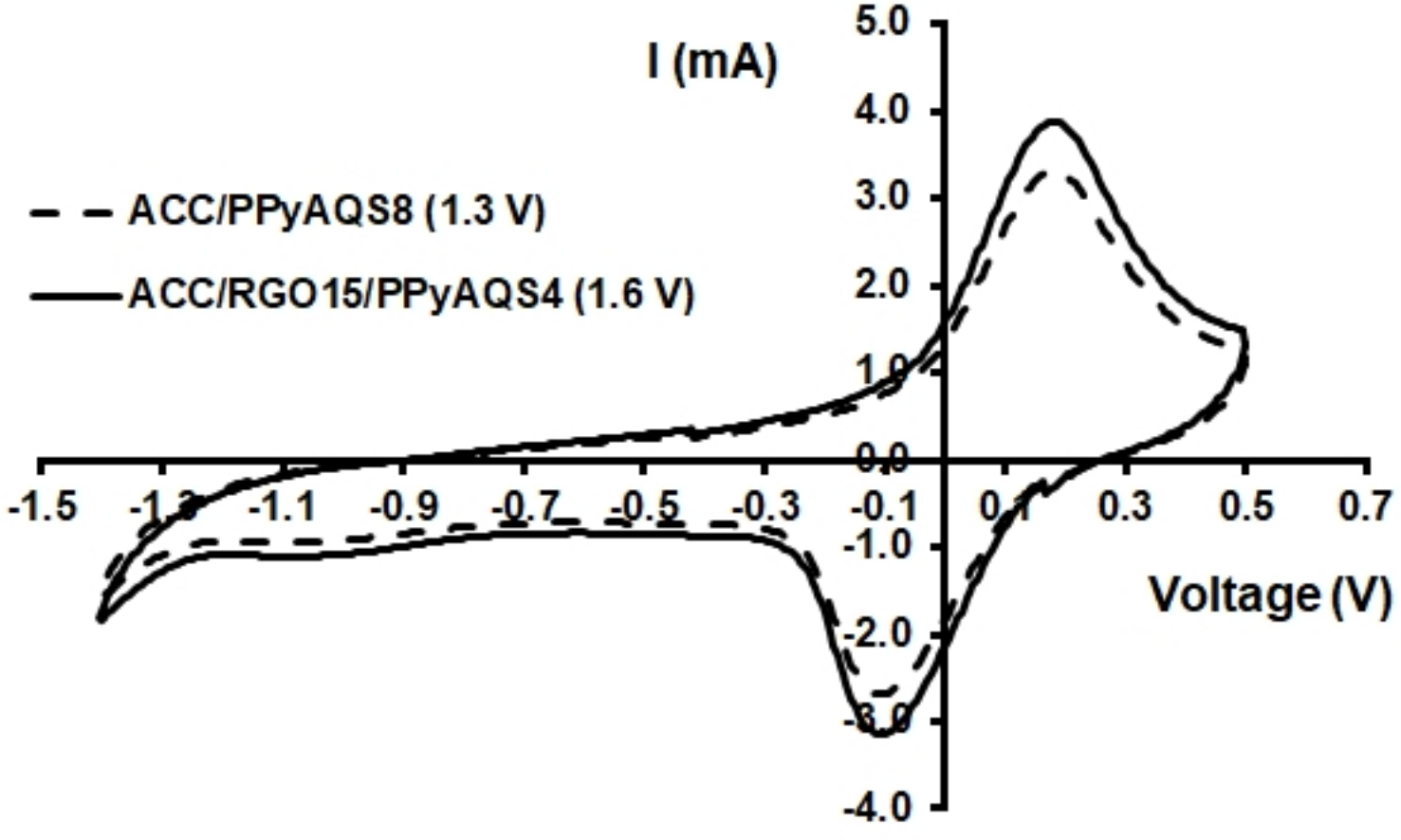
I (mA)
5.0
4.0
3.0
2.0
1.0
0.0
-1.0
-2.0
-3.0
-4.0
ACC/PPyAQS8 (1.3 V)
ACC/RGO15/PPyAQS4 (1.6 V)
-1.5
-1.1
-0.9
-0.7
-0.5
-0.3
-0.1
0.3
0.5
0.7
Voltage (V)

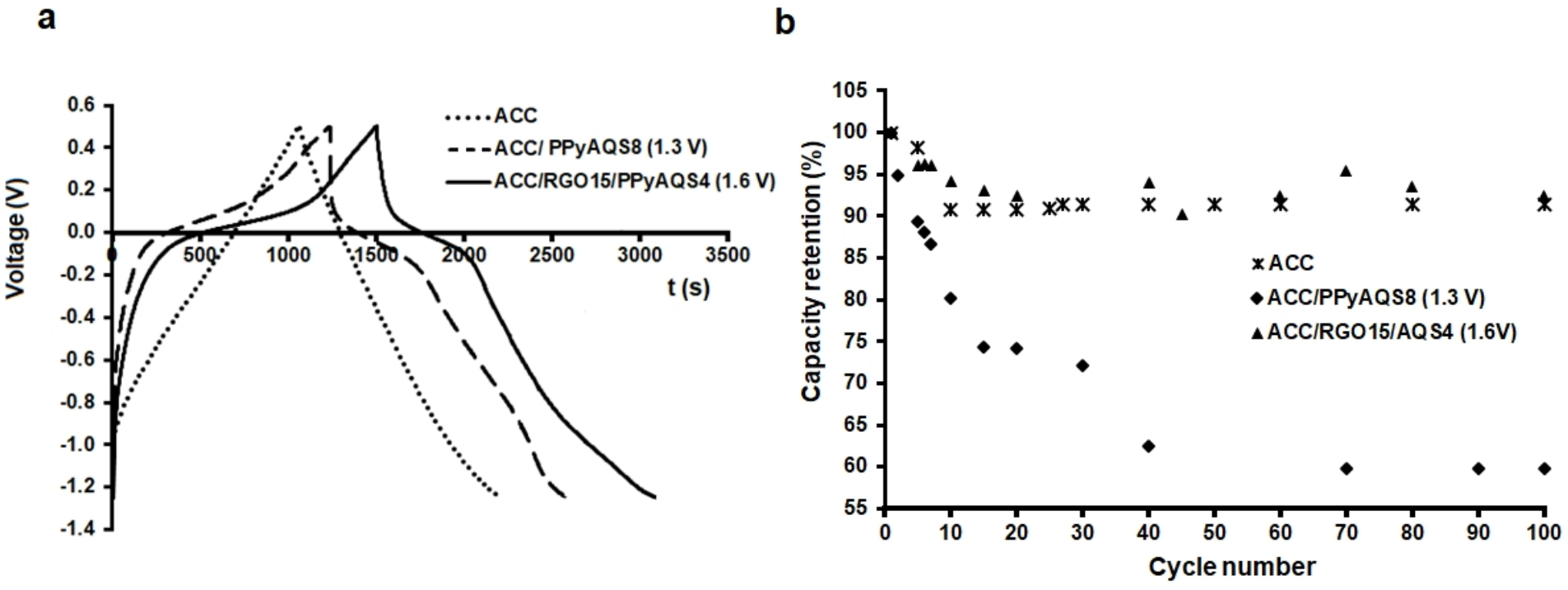
a
b
Voltage (V)
t (s)
ACC
ACC/ PPyAQS8 (1.3 V)
ACC/RGO15/PPyAQS4 (1.6 V)
1
Capacity retention (%)
Cycle number
ACC
ACC/PPyAQS8 (1.3 V)
ACC/RGO15/AQS4 (1.6V)

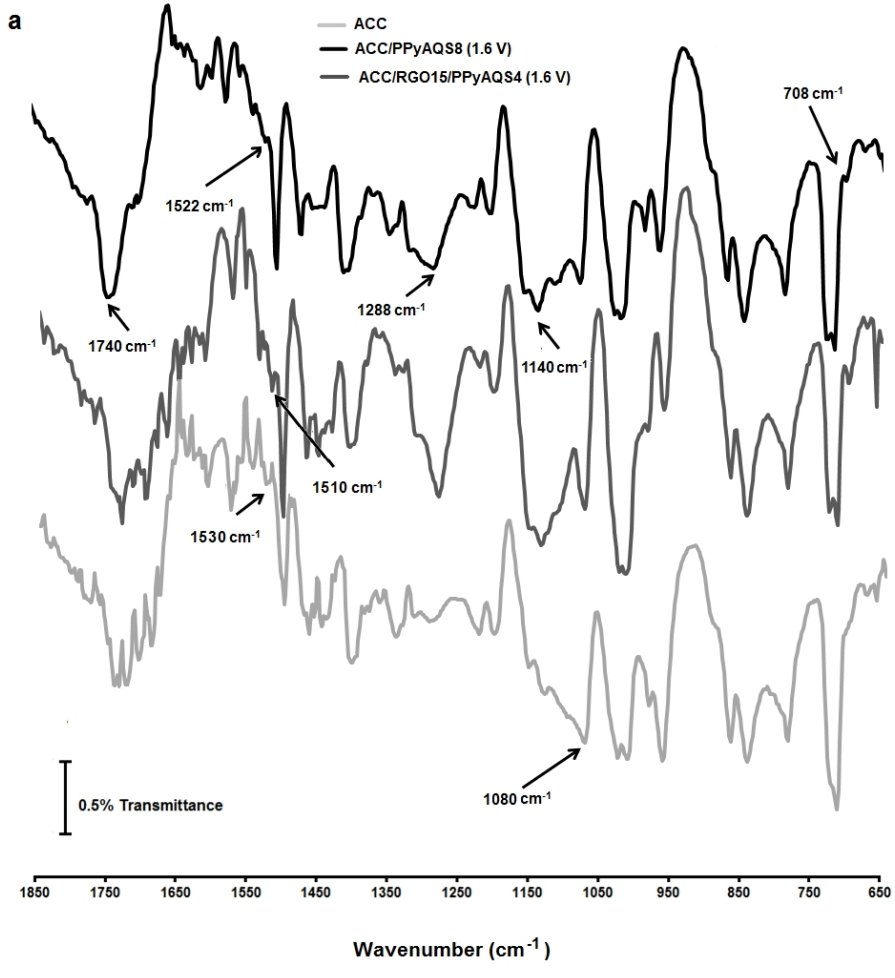
a
ACC
ACC/PPyAQS8 (1.6 V)
ACC/RGO15/PPyAQS4 (1.6 V)
1740 cm-1
1522 cm-1
1288 cm-1
1140 cm-1
708 cm-1
1510 cm-1
1530 cm-1
1080 cm-1
0.5% Transmittance
1850 1750 1650 1550 1450 1350 1250 1150 1050 950 850 750 650
Wavenumber (cm-1)

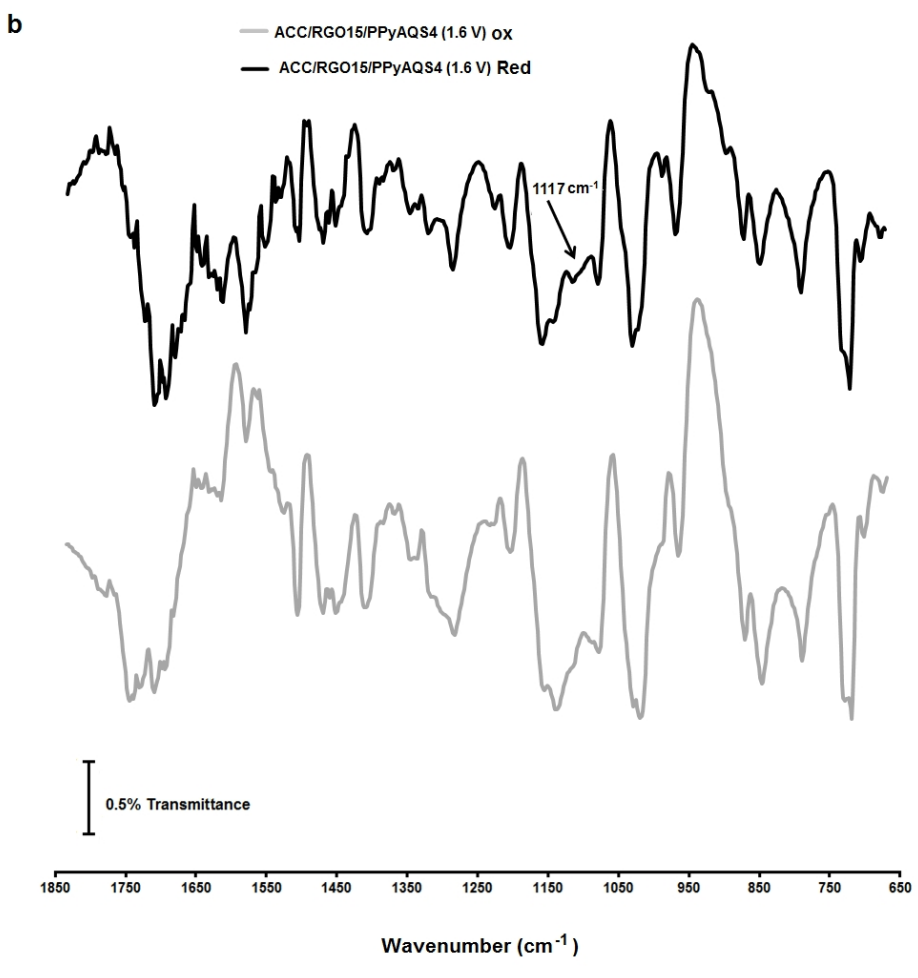
b
ACC/RGO15/PPyAQS4 (1.6 V) ox
ACC/RGO15/PPyAQS4 (1.6 V) Red
1117 cm-1
0.5% Transmittance
1850 1750 1650 1550 1450 1350 1250 1150 1050 950 850 750 650
Wavenumber (cm-1)